MICROBIOLOGY AND MOLECULAR BIOLOGY REVIEWS, Dec. 2011, p. 664–677 Vol. 75, No. 4
1092-2172/11/$12.00 doi:10.1128/MMBR.05008-11

Biosynthesis of the Metalloclusters of Molybdenum Nitrogenase

Yilin Hu* and Markus W. Ribbe*

University of California, Irvine, California

INTRODUCTION

Nitrogenases are a family of complex metalloenzymes that catalyze the reduction of atmospheric dinitrogen (N_2) to bioavailable ammonia (NH_3) in a nucleotide-dependent process (5, 22). Usually depicted as $N_2 + 8H^+ + 16MgATP + 8e^- \rightarrow 2NH_3 + H_2 + 16MgADP + 16P_i$, the reaction catalyzed by nitrogenases not only represents a key step in the global nitrogen cycle but also embodies the formidable chemistry of breaking the N≡N triple bond under ambient conditions. Because of these reasons, nitrogenase research has remained a focal point in the field of bioinorganic chemistry for decades.

So far, three homologous nitrogenases have been identified, which are mainly distinguished by the different types of heterometals (molybdenum [Mo], vanadium, or iron [Fe]) at their active sites (32). The Mo nitrogenase of *Azotobacter vinelandii* is one of the best-characterized members among these enzymes. It is a binary system comprising two component proteins. One, designated the Fe protein, is a homodimer that holds an [Fe_4S_4] cluster between the subunits and one ATP binding site per subunit. The other, designated the molybdenum iron (MoFe) protein, is an $\alpha_2\beta_2$-tetramer that contains two unique metalloclusters per αβ-dimer: a P-cluster ([Fe_8S_7]) at each α/β-subunit interface and a FeMo cofactor, or FeMoco ([$MoFe_7S_9X$-homocitrate]; X = C, N, or O), within each α-subunit (12, 35).

Catalysis of the Mo nitrogenase likely involves the complex formation between its two component proteins (47), in which the Fe protein serves as an ATP-dependent reductase, mediating the interprotein transfer of electrons from its [Fe_4S_4] cluster, through the P-cluster, to the FeMoco of the MoFe protein, where substrate reduction eventually occurs (Fig. 1). The distinctive structural and redox properties of the P-cluster and the FeMoco, therefore, underlie the unique reactivity of the MoFe protein, the catalytic component of the Mo nitrogenase.

* Corresponding author. Mailing address: 2236 McGaugh Hall, Department of Molecular Biology and Biochemistry, University of California, Irvine, CA 92687-3900. Phone: (949) 824-9509. Fax: (949) 824-8551. E-mail for Yilin Hu: yilinh@uci.edu. E-mail for Markus W. Ribbe: mribbe@uci.edu.

P-Cluster

The P-cluster can be viewed as a symmetrical double cubane in which two [Fe_4S_4] clusters share a sulfide atom in between (Fig. 2A and B). It is positioned at the interface between the α- and β-subunits of the MoFe protein, 10 Å below the surface of the protein (12, 35). In the presence of excess dithionite, the P-cluster exists in a diamagnetic state (designated the P^N state), where all of its Fe atoms are believed to be ferrous (52, 61). Following the treatment of indigodisulfonate (IDS), the P^N state can be two electron oxidized to a stable $S = 3$ or 4 state (designated the P^{OX} or P^{2+} state), which can be recognized by a $g = 11.8$ signal in parallel-mode electron paramagnetic resonance (EPR) spectroscopy (44, 52, 53). Both the P^N and P^{OX} states of the P-cluster (Fig. 2A and B) are covalently coordinated to the MoFe protein by three cysteinyl ligands from the α-subunit ($Cys^{\alpha62}$, $Cys^{\alpha88}$, and $Cys^{\alpha154}$) and three cysteinyl ligands from the β-subunit ($Cys^{\beta70}$, $Cys^{\beta95}$, and $Cys^{\beta153}$), with $Cys^{\alpha62}$, $Cys^{\alpha154}$, $Cys^{\beta70}$, and $Cys^{\beta153}$ each coordinating one Fe atom and $Cys^{\alpha88}$ and $Cys^{\beta95}$ each coordinating two Fe atoms of the P-cluster (6, 35, 42). However, the conversion of the P^N to the P^{OX} state results in a change in the core structure of the cluster, rendering one half of the cluster in a more open conformation (Fig. 2B). Moreover, such a structural rearrangement is accompanied by changes in the ligation between the cluster and the protein (42). Compared to the P^N state, the P^{OX} state is coordinated by two additional protein ligands: $Ser^{\beta188}$, which coordinates an Fe atom through an Oγ ligand along with the cysteinyl group of $Cys^{\beta153}$; and $Cys^{\alpha88}$, which coordinates an Fe atom through a backbone amide nitrogen ligand and a cysteinyl group (Fig. 2B).

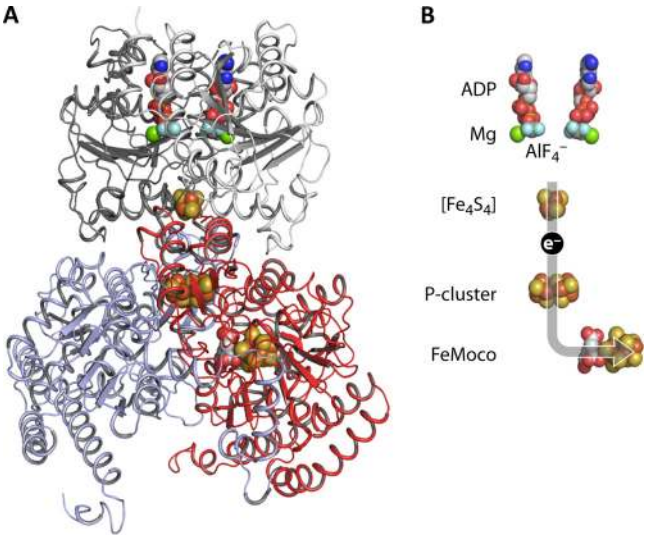

FIG. 1. Crystal structure of half of the ADP · AlF_4^--stabilized Fe protein/MoFe protein complex (A) and the relative positions of components involved in the electron flow (B). The two subunits of Fe protein are colored dark and light gray, and the α- and β-subunits of MoFe protein are colored red and blue, respectively. All clusters and ADP · AlF_4^- are shown as space-filling models, with the atoms colored as follows: Fe, orange; S, yellow; Mo, cyan; O, red; C, gray; N, dark blue; Mg, green; Al, beige; F, light blue. PYMOL was used to create the figure (PDB entry 1N2C).

FeMoco

The FeMoco can be viewed as an $[Fe_4S_3]$ and a $[MoFe_3S_3]$ cluster bridged by three inorganic sulfide atoms in between (Fig. 2C). It also contains an organic compound (homocitrate) at the Mo end, which has been implicated in the function of nitrogenase, and a μ_6-interstitial atom X (C, N, or O) in the center, which has promising relevance to the catalysis of nitrogenase (4, 12, 21, 35, 50). The FeMoco is buried within the α-subunit of MoFe protein, 14 Å away from the P-cluster. Unlike the subunit-bridging P-cluster, the FeMoco is ligated to the MoFe protein by only two ligands: $Cys^{\alpha 275}$, which coordinates the terminal Fe atom, and $His^{\alpha 442}$, which ligates the opposite Mo atom. A third residue, $Lys^{\alpha 426}$, provides an additional anchor for the homocitrate moiety at the Mo end (12). Such a ligation pattern permits the extraction of FeMoco as an intact entity into an organic solvent (for example, *N*-methylformamide [NMF]), which in turn facilitates the studies of both the protein-bound and the solvent-isolated forms of the cofactor (4, 50). The isolated FeMoco has been shown to be anionic (4), yet the proposed core charge of FeMoco in the resting state is +1 or +3 (37, 55). The overall negative charge of the cofactor, therefore, is believed to originate from its endogenous homocitrate moiety, which is −4 if the -OH group is deprotonated. The FeMoco displays a characteristic $S = 3/2$ EPR signal in the resting state; however, it can undergo a reversible one-electron oxidation and reduction process (5), which is accompanied by a change in the intensity of the $S = 3/2$ signal.

There is a substantial amount of interest in elucidating the biosynthetic mechanisms of the FeMoco and the P-cluster, because these clusters are not only biologically important but also chemically unprecedented. In the following sections, we review the recent advances in this research area, with an emphasis on our work that aims at providing structural and spectroscopic insights into the biosynthesis of the two complex metal clusters of *A. vinelandii* MoFe protein. An alternative view of certain aspects of FeMoco biosynthesis has been summarized elsewhere (46).

EX SITU ASSEMBLY OF FeMoco

Biosynthesis of FeMoco (Fig. 3) occurs independently of the production of the polypeptides of the target MoFe protein (hence the term "*ex situ* assembly"). It is arguably one of the most complex processes in bioinorganic chemistry, requiring, minimally, the participation of the gene products of *nifS*, *nifU*, *nifB*, *nifE*, *nifN*, *nifV*, and *nifH*. The hypothesized Fe and S "flow" in this process starts from NifS and NifU (encoded by *nifS* and *nifU*) and continues sequentially through NifB (encoded by *nifB*) and NifEN (encoded by *nifE* and *nifN*), during which process the Fe/S core structure of FeMoco is generated. The Fe protein (encoded by *nifH*)—the catalytic electron donor that is also crucial for FeMoco biosynthesis—"merges" onto such an Fe/S flow, which completes the maturation of the nascent FeMoco on NifEN. Once assembled, the FeMoco is

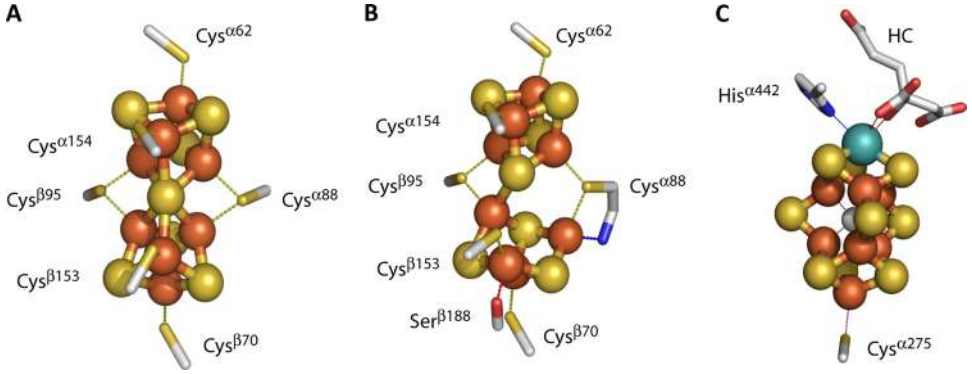

FIG. 2. Crystal structures of the P^N (A) and P^{OX} (B) states of the P-cluster and the FeMoco (C). The clusters are shown as ball-and-stick models, with the atoms colored as described in the legend to Fig. 1, and the ligands are shown in stick presentation. The interstitial atom X (C, N, or O) of FeMoco is colored gray in panel C. PYMOL was used to create the figure (PDB entries 1M1N and 3MIN). HC, homocitrate.

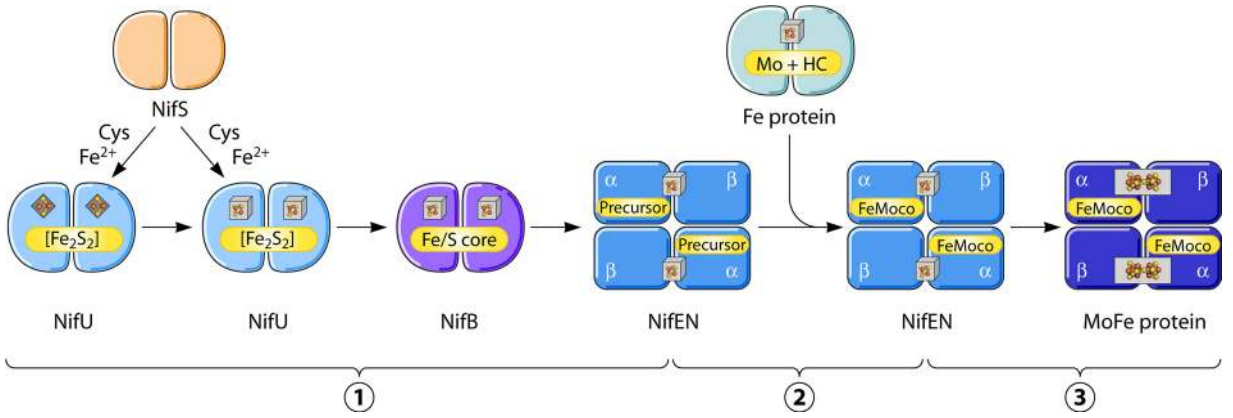

FIG. 3. Biosynthesis of FeMoco. NifS and NifU mobilize Fe and S for the sequential formation of $[Fe_2S_2]$ and $[Fe_4S_4]$ clusters, which are used as building blocks for the formation of a large Fe/S core on NifB. This Fe/S core is further processed into a molybdenum (Mo)- and homocitrate (HC)-free precursor, which can be converted to a mature FeMoco on NifEN upon Fe protein-mediated insertion of Mo and HC. Once the FeMoco is assembled on NifEN, it is delivered to its destined location in the MoFe protein. The permanent metal centers of the proteins are colored gray ($[Fe_2S_2]$ cluster, diamond; $[Fe_4S_4]$ cluster, cube; P-cluster, oval), and the transient cluster intermediates are colored yellow.

transferred from NifEN to the MoFe protein and inserted into its targeted binding site in the latter (49).

Formation of the Fe/S Core of FeMoco

The Fe/S core of FeMoco is presumably assembled by the combined action of NifS, NifU, and NifB before it is delivered to NifEN (Fig. 3, ①). Functioning as a pyridoxal phosphate-dependent cysteine desulfurase, NifS is responsible for the formation of a protein-bound cysteine persulfide that is subsequently donated to NifU for the sequential formation of $[Fe_2S_2]$ and $[Fe_4S_4]$ clusters (51). These small Fe/S clusters are then transferred to NifB and further processed into a large Fe/S core that likely contains all Fe and S necessary for the generation of a mature cofactor (1). The exact function of NifB in this process has long remained elusive; however, NifB is known to be indispensable for FeMoco assembly, as deletion of *nifB* results in the accumulation of a FeMoco-deficient form of MoFe protein (designated the Δ*nifB* MoFe protein) in *A. vinelandii* (48). Sequence analysis reveals that NifB has a CX XXCXXC signature motif at its N terminus, which is characteristic of a family of radical *S*-adenosyl-L-methionine (SAM)-dependent enzymes; additionally, NifB contains a sufficient amount of ligands for the coordination of the entire complement of the Fe atoms of FeMoco (49). Thus, the formation of Fe/S core on NifB may represent a novel synthetic route to bridged metal clusters that relies on radical chemistry at the SAM domain of NifB. Given that NifU likely donates $[Fe_4S_4]$ fragments to NifB for FeMoco assembly, it can be speculated that NifB tethers two $[Fe_4S_4]$ subclusters by an S atom and a light X (C, N, or O) atom, thereby generating a fully complemented Fe/S scaffold that could be rearranged into the core structure of FeMoco.

The initial support for the proposed role of NifB comes from the characterization of NifEN, the receiving end of the Fe/S core synthesized on NifB. A scaffold protein for the maturation of FeMoco, NifEN shares a significant degree of sequence homology with the MoFe protein. Such a sequence homology has led to the hypothesis that NifEN contains clusters analogous to the P-cluster and FeMoco in the MoFe protein (2). While the P-cluster analog in NifEN was established earlier as an $[Fe_4S_4]$ cluster (17), the FeMoco analog was captured only recently on a NifEN complex isolated from a *nifB*-intact yet *nifHDK*-deficient background of *A. vinelandii* (7, 28). The absence of the *nifDK*-encoded MoFe protein (the terminal acceptor of FeMoco) and the *nifH*-encoded Fe protein (an essential factor for FeMoco maturation) facilitates the accumulation of a FeMoco precursor on NifEN. Biochemical studies show that this precursor is free of Mo and homocitrate (28) and it can be converted to a mature cofactor upon the incorporation of the missing components by the Fe protein (see below). In the dithionite-reduced state, this precursor—together with the $[Fe_4S_4]$ clusters in NifEN—gives rise to a composite $S = 1/2$ signal (Fig. 4A, trace 1); whereas in the IDS-oxidized state, it contributes solely to a unique signal at $g = 1.94$ (Fig. 4B, trace 1) (28). Fe K-edge X-ray absorption spectroscopy (XAS) analyses of both the NifEN-bound (7) and the NMF-extracted (13) forms of the precursor define it as an 8Fe cluster that closely resembles the core structure of the mature FeMoco (Fig. 4D). The recently solved 2.6-Å crystal structure of the precursor-bound NifEN provides additional support to the extended X-ray absorption fine structure (EXAFS)-derived 8Fe model, showing that the electron density of the precursor is compatible in shape and extent with that of the core geometry of the mature cofactor (34). Together, these observations suggest that, instead of following the previously postulated mechanism that involves the coupling of $[Fe_4S_3]$ and $[MoFe_3S_3]$ subclusters, the FeMoco is assembled by having the complete Fe/S core structure in place before the insertion of Mo and homocitrate. Moreover, the high nuclearity of the NifEN-associated precursor points to a significant role of NifB, the biosynthetic apparatus immediately upstream of NifEN, in generating the complete Fe/S core of FeMoco.

Further insights into the function of NifB are afforded by the characterization of a NifEN-B fusion protein, an "integrated" assembly unit comprising two adjacent components along the biosynthetic pathway of FeMoco. Like the naturally fused *nifN* and *nifB* genes in *Clostridium pasteurianum*, the *nifN* and *nifB*

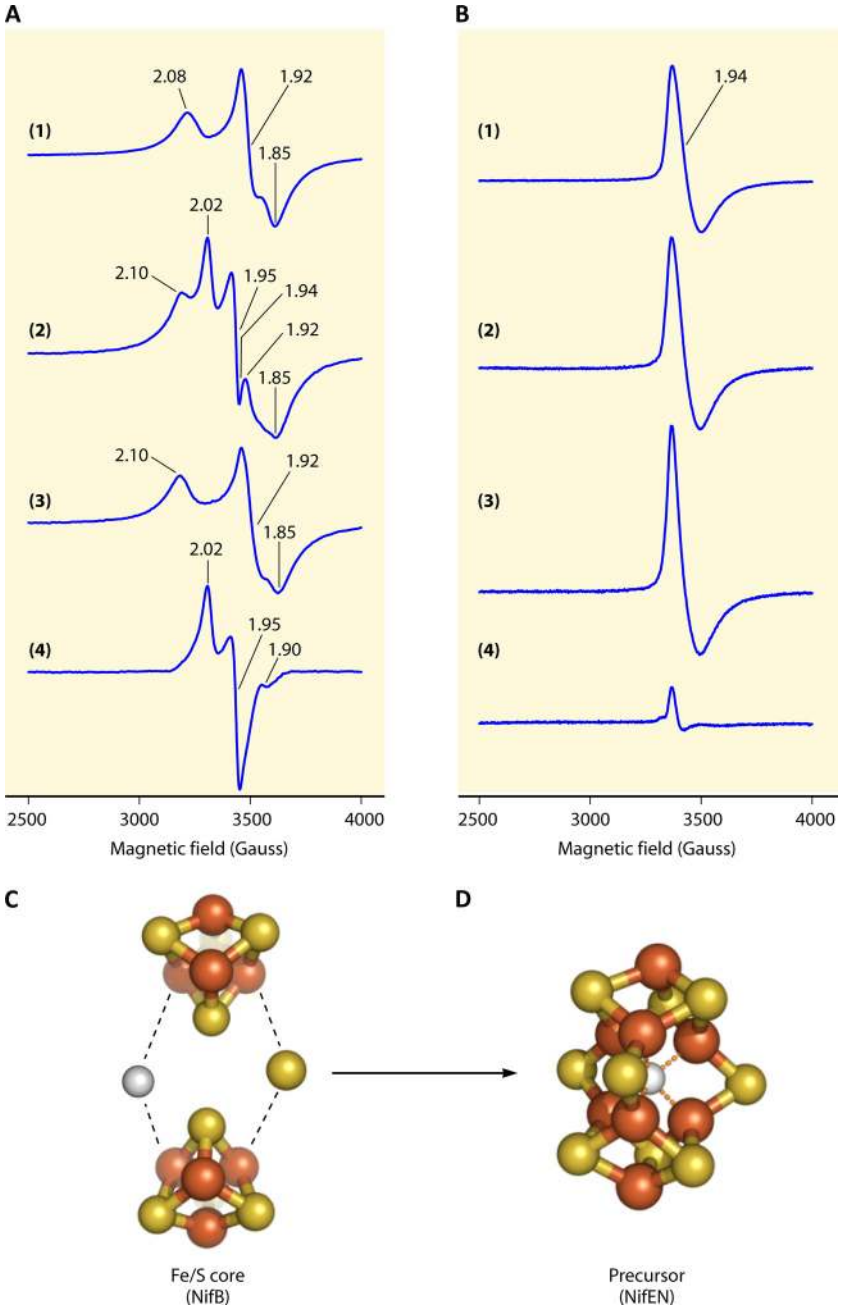

FIG. 4. (A and B) EPR spectra of dithionite-reduced (A) and IDS-oxidized (B) NifEN (trace 1) and NifEN-B in the absence (trace 2) and presence (trace 3) of 40 mM SAM. In the dithionite-reduced state, the precursor, together with the $[Fe_4S_4]$ clusters in NifEN, gives rise to a composite $S = 1/2$ signal at $g = 2.08$, 1.92, and 1.85 (A1), whereas in the IDS-oxidized state, the precursor contributes solely to a unique $g = 1.94$ signal (B1). Subtraction of the dithionite-reduced spectrum of NifEN-B plus SAM (A3) from that of NifEN-B (A2) results in an $S = 1/2$ signal at $g = 2.02$, 1.95, and 1.90 (A4), which is associated with the $[Fe_4S_4]$-type clusters in the NifB entity of NifEN-B. Subtraction of the IDS-oxidized spectrum of NifEN-B (B2) from that of NifEN-B plus SAM (B3) results in a $g = 1.94$ signal, which represents the newly generated 8Fe precursor in the NifEN entity of NifEN-B. (C and D) Conversion of 4Fe intermediates on NifB (C) into an 8Fe precursor that appears on NifEN (D). NifB could bridge two $[Fe_4S_4]$ clusters while inserting an S atom along with the interstitial X atom (C, N, or O) in a SAM-dependent mechanism, thereby generating an Fe/S core, which could be rearranged into a precursor that closely resembles the core structure of the mature FeMoco. The clusters are shown as ball-and-stick models, with the atoms colored as in Fig. 1. PYMOL was used to create the figure.

genes of *A. vinelandii* can be fused together and expressed homologously in a *nifHDK* deletion background of *A. vinelandii* (54). Like NifEN, NifEN-B is a heterotetramer with a subunit composition of $NifE_2(N\text{-}B)_2$. In the IDS-oxidized state, NifEN-B displays a $g = 1.94$ EPR signal (Fig. 4B, trace 2) that is characteristic of the NifEN-associated precursor (Fig. 4B, trace 1), suggesting that, like NifEN, NifEN-B accumulates the same 8Fe precursor as a result of the *nifHDK* deletion (see

above). In the dithionite-reduced state, however, NifEN-B exhibits extra EPR features (Fig. 4A, trace 2) that overlap with the $S = 1/2$ signal typically displayed by NifEN (Fig. 4A, trace 1), suggesting that, compared to NifEN, NifEN-B contains additional cluster species as a result of the *nifN-nifB* fusion. Interestingly, these extra EPR features respond dramatically to SAM, showing a decrease in magnitude that eventually leads to their disappearance at 40 mM SAM (Fig. 4A, trace 3). Subtraction of the spectrum of NifEN-B (plus SAM) from that of NifEN-B (without SAM) reveals that these SAM-responsive features belong to a distinctive $S = 1/2$ signal ($g = 2.02$, 1.95, and 1.90), which can be attributed to the presence of $[Fe_4S_4]$-type clusters at/near the SAM-binding domain of the NifB entity (Fig. 4A, trace 4). Quantitative EPR, UV/visible and metal analyses further suggest that, apart from the two SAM-motif-bound $[Fe_4S_4]$ clusters, there are additional $[Fe_4S_4]$ clusters—likely located near the SAM motif—which could represent the NifB-bound intermediate of FeMoco assembly (54). This argument is supported by the observation of the concurrent disappearance of both SAM-motif- and non-SAM-motif-associated signals (Fig. 4A, trace 4) and the increased magnitude of the precursor-specific signal (Fig. 4B, trace 4), as well as the increased capacity of NifEN-B as a FeMoco donor (54), upon the addition of SAM. Taken together, these results strongly indicate that NifB houses the assembly of an 8Fe precursor (Fig. 4D) from small $[Fe_4S_4]$ fragments (Fig. 4C) in a SAM-dependent mechanism.

Insertion of Mo and Homocitrate into the Fe/S Core

The 8Fe precursor can be transformed, while it is bound to NifEN, into a mature cofactor in an *in vitro* maturation assay containing dithionite, Fe protein, MgATP, molybdate (MoO_4^{2-}), and homocitrate (Fig. 3, ②). Under *in vivo* conditions, the homocitrate is supplied by NifV (encoded by *nifV*), which is responsible for the synthesis of this organic compound (20, 60), and the Mo is likely mobilized by other carrier/storage proteins prior to the intervention of Fe protein (18, 33), although the Fe protein is the only protein that has been directly linked in this capacity to the assembly of FeMoco (23, 24, 56). Upon maturation, the precursor-specific $g = 1.92$ signal disappears in the IDS-oxidized spectrum of NifEN (Fig. 5B, trace 1), whereas a small, FeMoco-like signal appears at $g = 4.45$, 3.96, 3.60, and 2.03 in the dithionite-reduced spectrum of NifEN (Fig. 5B, trace 2). Fe and Mo K-edge XAS/EXAFS analyses (23, 56) reveal that the FeMoco formed on NifEN is nearly identical in structure to the mature cofactor in MoFe protein (Fig. 5D), although the coordination of Mo is somewhat asymmetric due to a different ligand environment at the Mo end of the cofactor. The hydrolysis of ATP is absolutely required for the maturation of precursor on NifEN, as this process cannot occur if ATP is substituted with ADP or nonhydrolyzable ATP analogs or if the wild-type Fe protein is replaced by Fe protein variants that are defective in MgATP hydrolysis (23, 24). Additionally, there is a clear dependence of maturation efficiency on redox potential, as an increase of dithionite concentration from 2 to 20 mM leads to an increase of cofactor maturation by 3- to 4-fold (56). As the Fe protein is the only known ATP-dependent reductase in the *in vitro* maturation assay, the ATP and redox dependence of cofactor maturation suggests a crucial role of the Fe protein in this process.

Subsequent analyses of the Fe protein reisolated from the *in vitro* maturation assay show that it is "loaded" with Mo and homocitrate, and it can directly serve as the donor of these two components to the precursor on NifEN (24). Mo K-edge XAS analysis of the loaded Fe protein demonstrates a decrease in the number of Mo=O bonds (two or three instead of the four in MoO_4^{2-}) and the effective oxidation state of Mo, which could result from a change in the formal oxidation state and/or the ligation pattern of Mo. Interestingly, the EPR spectrum of the loaded Fe protein has an intermediary line shape between those of the spectra of the MgADP- and MgATP-bound forms of Fe protein (24). This observation coincides with that from the initial structural analysis of an ADP-bound form of Fe protein, which reveals that Mo occupies a position that corresponds to the γ-phosphate of ATP (16). Considering the structural similarity between phosphate and molybdate, such an ADP-Mo binding pattern may very well represent the first step of Mo mobilization by Fe protein during the FeMoco maturation process. As far as homocitrate is concerned, there is evidence that this organic compound is mobilized together with Mo by the Fe protein for the maturation of FeMoco. NifEN reisolated from an incomplete homocitrate-free maturation assay carries a homocitrate-deplete yet Mo-replete cluster (designated the FeMo cluster) that cannot be further matured into FeMoco even upon the supplementation of homocitrate, suggesting that homocitrate is delivered simultaneously with Mo to the NifEN-associated precursor (14). Additionally, the Mo K-edge XAS spectrum of the Mo-bound Fe protein displays a clear edge shift from that of the Mo- and homocitrate-bound Fe protein, further illustrating the coattachment of Mo and homocitrate to the Fe protein and, consequently, the comobilization of these components for the maturation of the precursor on NifEN (24).

A second role can be proposed for the Fe protein based on these observations, one in the capacity of a Mo/homocitrate insertase for the maturation of precursor on NifEN. To carry out this function, the Fe protein likely interacts with NifEN in a process that parallels the interaction between the Fe protein and the MoFe protein during catalysis (Fig. 1). Apart from sharing the ATP- and redox-dependent features, the two processes are connected by the structural homology between NifEN and the MoFe protein. Crystallographic analysis confirms that NifEN is highly homologous to the MoFe protein in the overall conformation (Fig. 6A); more excitingly, it reveals a nearly surface-exposed location of the NifEN-associated precursor (Fig. 6B), which is poised to be transformed into a mature cofactor upon the Fe protein-mediated insertion of Mo and homocitrate (34).

Transfer of FeMoco to Its Binding Site

Once a fully matured cofactor is formed on NifEN, it is delivered from its assembly site in NifEN to its binding site in the MoFe protein (Fig. 3, ③). The recent observation that such a transfer can be accomplished upon direct protein-protein interactions between NifEN and the MoFe protein (23), along with the previous documentation of unaffected nitrogen-fixing capability of the host upon the deletion of potential carrier-encoding gene(s) (11), precludes the absolute requirement of FeMoco carriers between the two proteins.

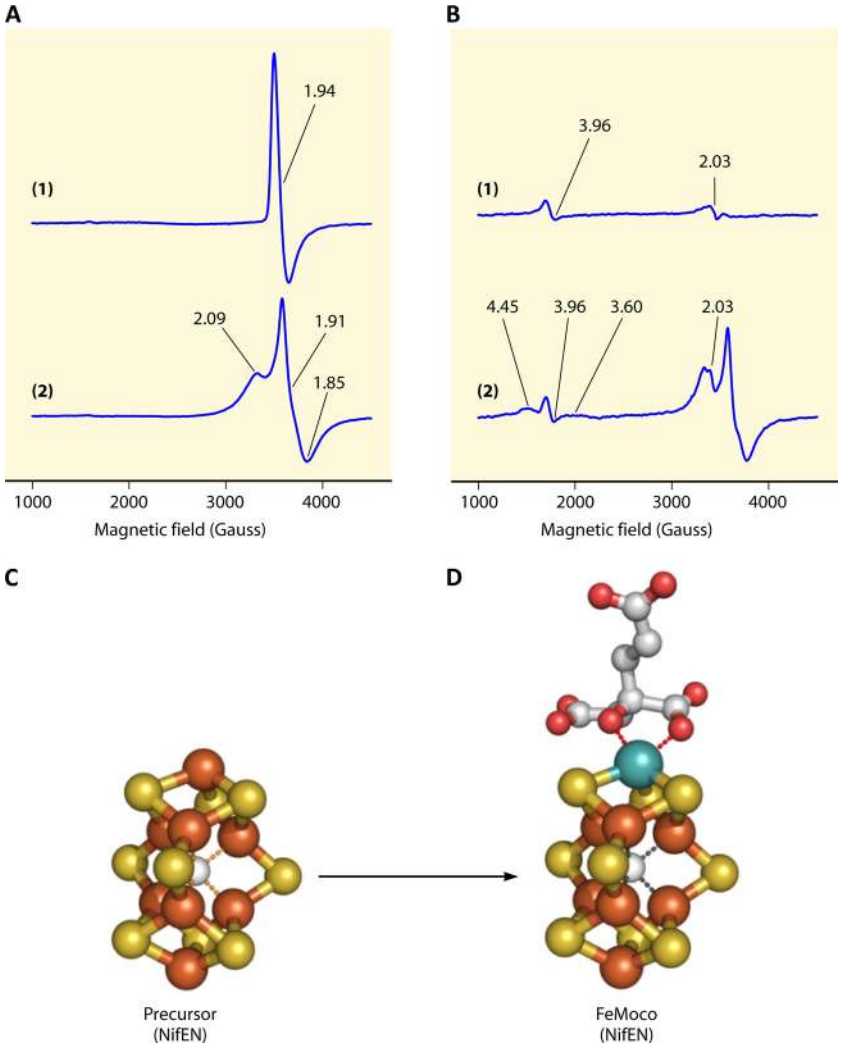

FIG. 5. (A and B) EPR spectra of precursor (A)- and FeMoco (B)-bound NifEN in the IDS-oxidized (trace 1) and dithionite-reduced (trace 2) states. In the IDS-oxidized state, the precursor-specific $g = 1.94$ signal (A1) disappears upon Mo and homocitrate incorporation (B1), whereas two small features appear at $g = 3.96$ and 2.03 (B1). In the dithionite-reduced state, a FeMoco-like signal emerges at $g = 4.45$, 3.96, 3.60, and 2.03 following such a transformation (B2), whereas the $S = 1/2$ signal (A2) reduces in amplitude (B2) due to the disappearance of the precursor-associated portion of this signal (28). (C and D) Conversion of an 8Fe precursor (C) into a mature FeMco on NifEN (D). The 8Fe precursor is an all-Fe homolog of FeMoco, which closely resembles the core structure of a mature FeMoco. Such a precursor can be transformed, while bound to NifEN, to a fully assembled FeMoco upon incubation with the Fe protein, MgATP, dithionite, MoO_4^{2-}, and homocitrate. The clusters are shown as ball-and-stick models, with the atoms colored as in Fig. 1. PYMOL was used to create the figure.

The completion of FeMoco assembly on NifEN triggers the docking of NifEN on the MoFe protein. Unlike the precursor-bound NifEN, the FeMoco-bound NifEN is capable of forming a complex with the MoFe protein, suggesting that the maturation of FeMoco is accompanied by a conformational change of NifEN that is required for the association between NifEN and the MoFe protein, as well as the subsequent transfer of the cofactor from the former to the latter (14). Interestingly, the insertion of Mo alone into the precursor is sufficient to induce a conformational change of NifEN, as the FeMo cluster-bound NifEN (see above) can also form a complex with the MoFe protein. However, the homocitrate-free FeMo cluster cannot be subsequently transferred to the MoFe protein, suggesting that the negatively charged homocitrate moiety plays an indispensable role in inserting the cofactor into the MoFe protein (14). Comparison between the primary sequences of NifEN and MoFe protein leads to the proposal that the two proteins contain similar cofactor-binding sites, yet it also reveals that certain residues of MoFe protein that either provide a covalent ligand to the FeMoco or tightly pack the FeMoco within the polypeptide matrix are not duplicated in the sequence of NifEN (49). Thus, it is possible that the respective cluster-binding sites in NifEN and MoFe protein are brought in close proximity upon complex formation between the two proteins, which allows the FeMoco to "diffuse" from the transient assembly site in NifEN (low-affinity site) to the final binding site in the MoFe protein (high-affinity site).

The presence of an analogous cofactor-binding site in NifEN is substantiated by the crystallographic analysis of the precursor-bound form of NifEN (34). Like the MoFe protein, NifEN

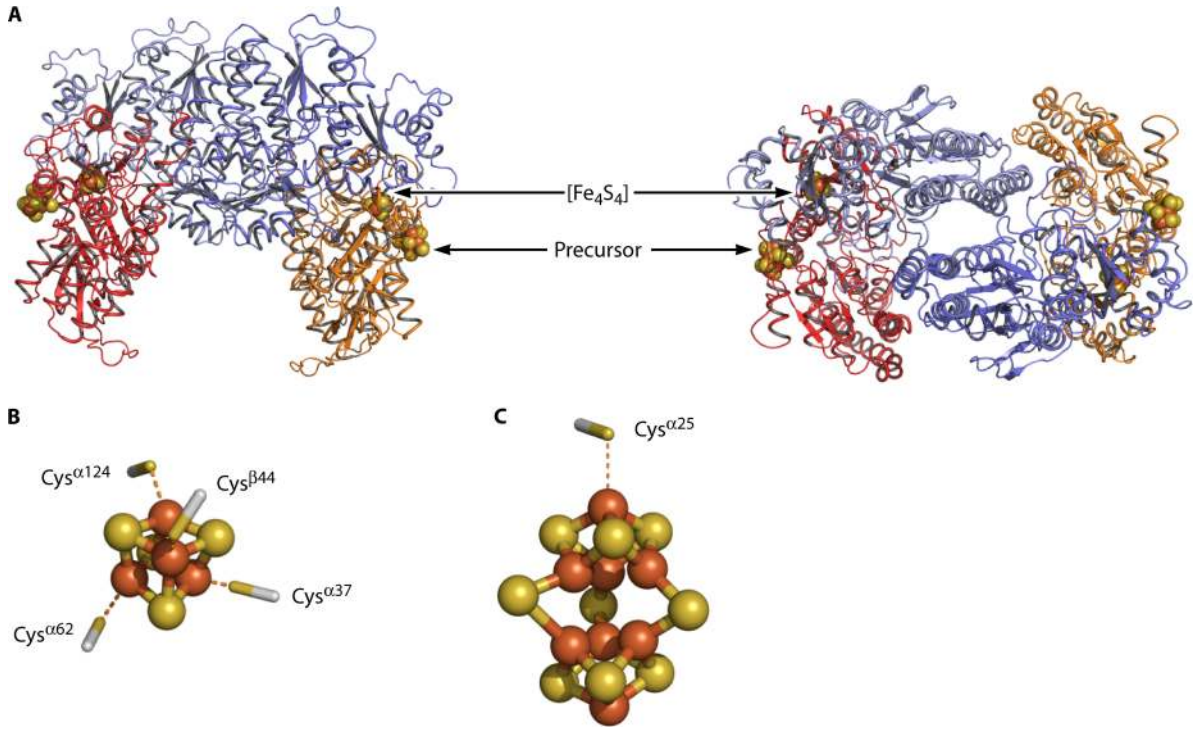

FIG. 6. (A) Structure of the NifEN tetramer with the molecular 2-fold axis oriented vertically (left) and along the viewing direction (right). The α-subunits are colored red and yellow, and the β-subunits are colored light and dark blue. (B and C) Structures and ligands of the $[Fe_4S_4]$ cluster (P-cluster analog) (B) and the 8Fe precursor (FeMoco analog) (C). Both clusters are shown as ball-and-stick models, with the atoms colored as in Fig. 1, and the ligands are shown in stick presentation. PYMOL was used to create the figure (PDB entry 3PDI).

consists of a pair of αβ-dimers that are related by a molecular 2-fold rotation axis (Fig. 6A). The α- and β-subunits of NifEN, as for the MoFe protein, is composed of three domains each: αI, αII, and αIII and βI, βII, and βIII, respectively. All of these domains are organized around a common core of a four-stranded parallel β-sheet, which is flanked with α-helices and additional β-strands (Fig. 6A). Apart from sharing a highly homologous conformation with the MoFe protein, NifEN also contains two clusters that are analogous to those found in the wild-type MoFe protein: an $[Fe_4S_4]$ cluster (P-cluster analog), which is coordinated by four cysteinyl ligands ($Cys^{\alpha37}$, $Cys^{\alpha62}$, $Cys^{\alpha124}$, and $Cys^{\beta44}$) at the α/β-subunit interface (Fig. 6B), and an Fe-only precursor (FeMoco analog), which is ligated to the α-subunit by at least one cysteinyl ligand ($Cys^{\alpha25}$) at one end (Fig. 6C). Strikingly, although the precursor and the FeMoco are both located at the junction between the αI, αII, and αIII domains of their respective host proteins, the precursor in NifEN is nearly surface exposed, shielded from the solvent by only a small stretch of disordered polypeptide (between residues α14 and α24) (Fig. 7B), whereas the FeMoco in the wild-type MoFe protein is buried within, approximately 10 Å below the surface of the protein (Fig. 7C). In the case of the Δ*nifB* MoFe protein, an open path is created due to the absence of FeMoco, which leads all the way from the surface of the MoFe protein to the FeMoco-binding site within the protein (Fig. 7A). Given the significant homology between NifEN and the MoFe protein, it is likely that upon maturation, the FeMoco is transferred from the surface to a site within the NifEN that is analogous to the FeMoco binding site within the wild-type MoFe protein. The conformational change of NifEN following the conversion of precursor to FeMoco, suggested by the ability of NifEN to complex with the MoFe protein upon such a transformation, lends further support to this hypothesis (14).

Overall, the α-subunit of NifEN assumes a conformation that is more open than that of the wild-type MoFe protein yet less open than the Δ*nifB* MoFe protein. Since the FeMoco-deficient and FeMoco-bound forms of the MoFe protein are respectively analogous to the precursor-free and FeMoco-bound forms of NifEN—the snapshots before and after the precursor-bound form of NifEN along the FeMoco assembly pathway—the varying degrees of openness in these structures imply that the α-subunit undergoes major structural rearrangements upon the maturation of precursor on NifEN. Indeed, a closer examination of the molecular surfaces of these proteins reveals the presence of a positively charged funnel in the Δ*nifB* MoFe protein, which could accommodate the insertion of the negatively charged FeMoco through charge-charge interactions (Fig. 7D). Such an insertion funnel is closed up in the wild-type MoFe protein, which may reflect a conformational change that occurs upon the incorporation of the FeMoco (Fig. 7F). In the case of NifEN, while there is an accumulation of positive surface charge that is similar to that observed for the Δ*nifB* MoFe protein, an insertion funnel could not be clearly defined (Fig. 7E). The docking of the precursor on the surface may have caused a partial closure of the funnel, rendering the NifEN in an intermediary conformation between the Δ*nifB* and

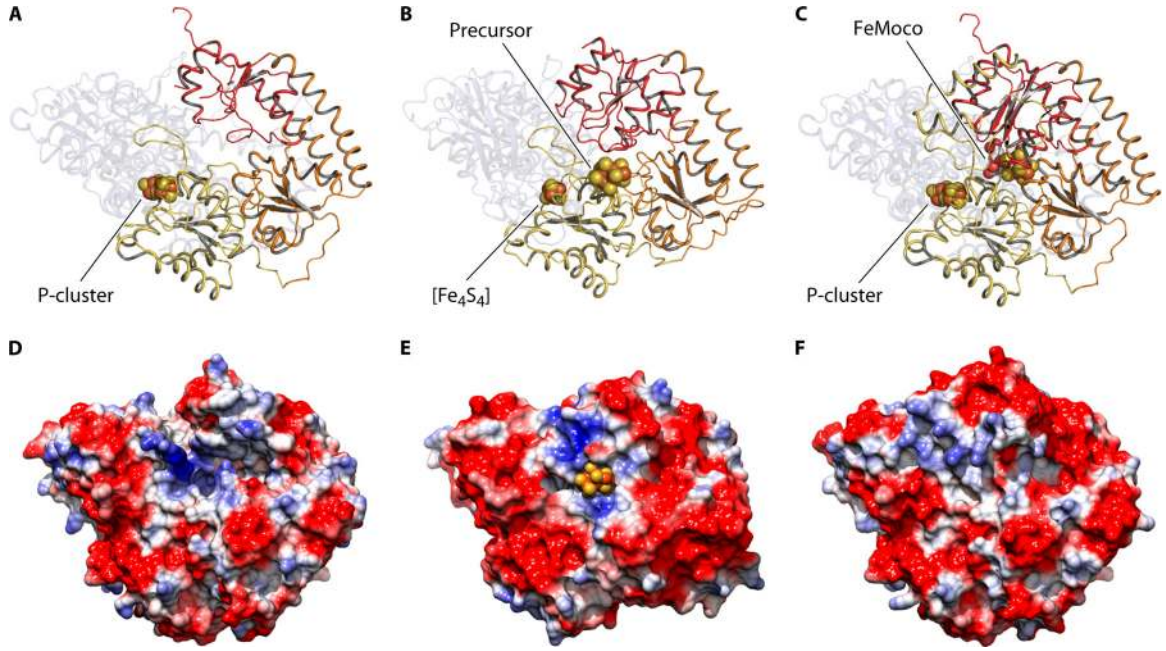

FIG. 7. Structures of the αβ-dimers of the Δ*nifB* MoFe protein (A), NifEN (B), and the wild-type MoFe protein (C). The α-subunits are presented in the foreground, and the β-subunits are rendered transparent in the background. The domains of the α-subunits are colored yellow (αI), orange (αII), and red (αIII), and the β-subunits are colored blue. Electrostatic surface potential representations of the αβ-dimers of the Δ*nifB* MoFe protein (D), NifEN (E), and the wild-type MoFe protein (F). Negative and positive potentials are colored red and blue, respectively. All clusters are shown as space-filling models, with the atoms colored as in Fig. 1. PYMOL and CHIMERA (43) were used to prepare the figure (PDB entries 1M1N, 1L5H, and 3PDI).

wild-type MoFe protein and, by analogy, the precursor-free and FeMoco-bound NifEN.

A common pathway of cluster insertion can be proposed for NifEN and MoFe protein on the basis of these analyses, which involves the generation of a precursor- or FeMoco-deficient protein that contains an open insertion funnel, the docking of the cluster at the entrance of the funnel, and the subsequent insertion of the cluster into the funnel (Fig. 8). The two path-

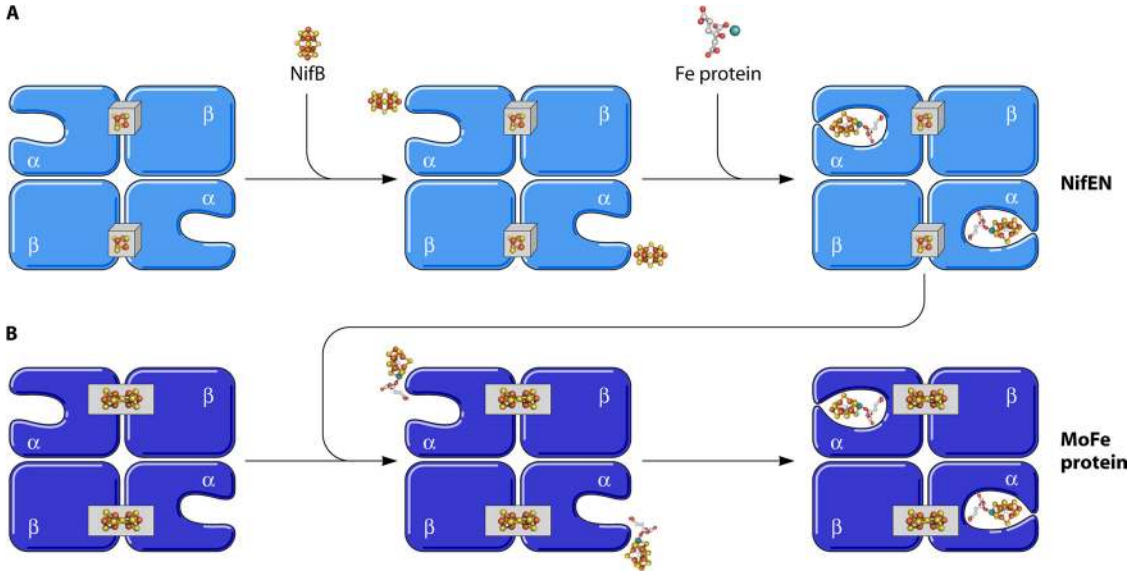

FIG. 8. Transfer of FeMoco to its binding site. (A) Following the synthesis of a [Fe_4S_4]-cluster-containing yet precursor-deficient form of NifEN (left), the precursor is delivered from NifB to the entrance of the cluster insertion funnel in NifEN (middle). Subsequently, the Fe protein inserts molybdenum (Mo) and homocitrate (HC) into the precursor, resulting in a mature FeMoco that is transferred to its binding site in NifEN (right). (B) The MoFe protein first appears as a P-cluster-containing yet FeMoco-deficient form (left). Upon direct protein-protein interactions, the mature FeMoco is transferred from NifEN to the entrance of the cluster insertion funnel in the MoFe protein (middle). Subsequently, the FeMoco is inserted into its binding site in the MoFe protein (right). The proposed biosynthetic events on NifEN mirror those on the MoFe protein, which is consistent with the significant homology between the overall structure and the cluster topology of the two proteins. The permanent metal centers of the proteins are colored gray ([Fe_4S_4] cluster, cube; P-cluster, oval). PYMOL was used to create the figure.

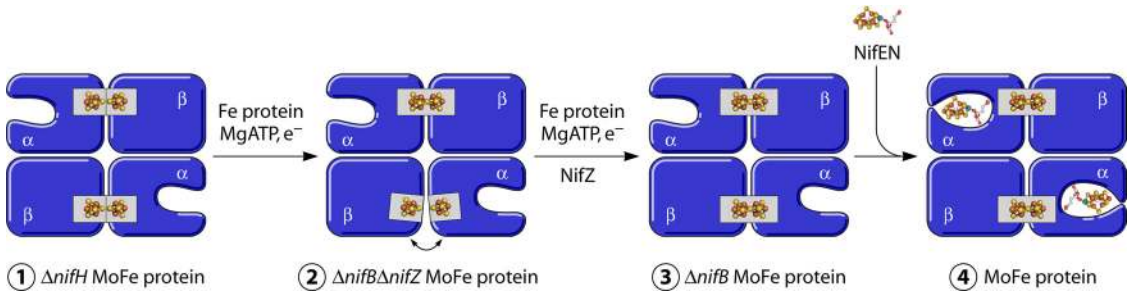

FIG. 9. Biosynthesis of P-cluster. The $[Fe_8S_7]$ P-cluster is assembled through the fusion of paired $[Fe_4S_4]$ clusters at the α/β-subunit interface. The two P-clusters in MoFe protein are assembled sequentially: the formation of the first P-cluster involves the sole action of Fe protein, whereas the formation of the second P-cluster requires the concerted action of Fe protein and NifZ. As a result of the stepwise assembly of P-clusters, the two αβ-dimers of the MoFe protein are assembled one at a time. Moreover, formation of the P-cluster at the α/β-subunit interface not only provides added stability to each αβ-dimer but also induces a conformational change that "opens" up the FeMoco site, thereby allowing the incorporation of the cofactor and the completion of the assembly process of MoFe protein. The different conformations of MoFe protein along the biosynthetic pathway are represented by the following: ①, the Δ*nifH* MoFe protein, which contains two $[Fe_4S_4]$ cluster pairs, one per αβ-dimer; ②, the Δ*nifB* Δ*nifZ* MoFe protein, which contains one P-cluster in one αβ-dimer and one $[Fe_4S_4]$ cluster pair in the other αβ-dimer; ③, the Δ*nifB* MoFe protein, which contains two P-clusters, one per αβ-dimer; and ④, the wild-type MoFe protein, which contains two complete sets of P-cluster and FeMoco, one set per αβ-dimer.

ways are connected through the interaction between NifEN and MoFe protein, which likely leads to a conformational change of NifEN that facilitates the release of FeMoco from its transient binding site and the movement of the cofactor back to the surface of NifEN. Subsequently, the FeMoco is transferred from the surface of NifEN to the surface of the MoFe protein, likely through the coordination of corresponding ligands—for example, the $Cys^{\alpha 25}$ that ligates the precursor in NifEN and, likewise, the corresponding $Cys^{\alpha 45}$ of the MoFe protein—which could tether and facilitate the efficient intermolecular transfer of FeMoco between the surfaces of the two proteins without the cofactor escaping to the surrounding environment.

Once it reaches the surface of the MoFe protein, the FeMoco interacts with a number of MoFe protein residues en route to its final binding site. Located in three key regions along the insertion funnel of the Δ*nifB* MoFe protein, these residues include (i) the "lid loop" residues (α353 to α364, with $His^{\alpha 362}$ at the tip of the loop), which could serve as transient ligands for the FeMoco at the entrance of the funnel; (ii) the "His triad" residues ($His^{\alpha 274}$, $His^{\alpha 442}$, and $His^{\alpha 451}$), which may provide a midway docking point for the FeMoco in the funnel; and (iii) the "switch/lock" residues ($His^{\alpha 442}$ and $Trp^{\alpha 444}$), which could lock the FeMoco in its binding site through the bulky side chain of $Trp^{\alpha 444}$ following a switch in position between $Trp^{\alpha 444}$ and $His^{\alpha 442}$ (48). Mutational analyses support the proposed roles of these residues, showing specifically decreased levels of FeMoco incorporation upon removal of the positive charge, the ligand capacity, and the steric effect at these positions (15, 29, 30). The insertion of FeMoco is accompanied by a significant conformational rearrangement of the MoFe protein. Small-angle X-ray scattering (SAXS) analyses indicate that the Δ*nifB* MoFe protein has a more extended conformation than its wild-type counterpart (8). Given that the Δ*nifB* MoFe protein represents the biosynthetic intermediate right before the wild-type MoFe protein, this observation suggests that the MoFe protein is compacted upon the insertion of FeMoco.

IN SITU ASSEMBLY OF P-CLUSTER

Biosynthesis of the P-cluster (Fig. 9), like that of FeMoco, starts with the actions of NifS and NifU. However, further processing of the small, NifU/NifS-generated Fe/S fragments into a mature P-cluster takes place within the target MoFe protein (hence the term "*in situ* assembly"). Fe protein and NifZ (encoded by *nifZ*) are two key players in this process, which in turn coordinates the assembly of the two αβ halves of the MoFe protein and the insertion of FeMoco into the protein (27).

Reductive Coupling of Paired $[Fe_4S_4]$ Subclusters into a P-Cluster

The symmetrical geometry of the $[Fe_8S_7]$ P-cluster, as well as the recovery of $[Fe_4S_4]$ fragments from earlier P-cluster extraction attempts (22), suggests that the P-cluster is likely assembled by the fusion of two $[Fe_4S_4]$-like subclusters. Such a reaction mechanism has been well established in synthetic chemistry (38) and successfully realized by the recent synthesis of P-cluster topologs (19, 40, 41, 57, 59). The biological evidence in this regard was supplied by the characterization of a MoFe protein isolated from the *nifH* deletion background of *A. vinelandii* (designated the Δ*nifH* MoFe protein). Like the Δ*nifB* MoFe protein, the Δ*nifH* MoFe protein is FeMoco deficient due to the absence of Fe protein, an essential factor for FeMoco maturation (45). However, contrary to the Δ*nifB* MoFe protein, the Δ*nifH* MoFe protein contains an unusual P-cluster, displaying, in the dithionite-reduced state, an $S = 1/2$ EPR signal that is characteristic of $[Fe_4S_4]^{1+}$ clusters (Fig. 10A, trace 1). Fe K-edge XAS/EXAFS analyses (9, 36) reveal that the P-cluster in the Δ*nifH* MoFe protein is composed of a pair of unbridged $[Fe_4S_4]$-like clusters: one of them has the standard $[Fe_4S_4]$ architecture, whereas the other is distorted (for example, with a core sulfide replaced by a bridging Cys) and/or coordinated by additional light atoms (such as N or O from Asp, His, Ser, or adventitious water) (Fig. 10C). Magnetic

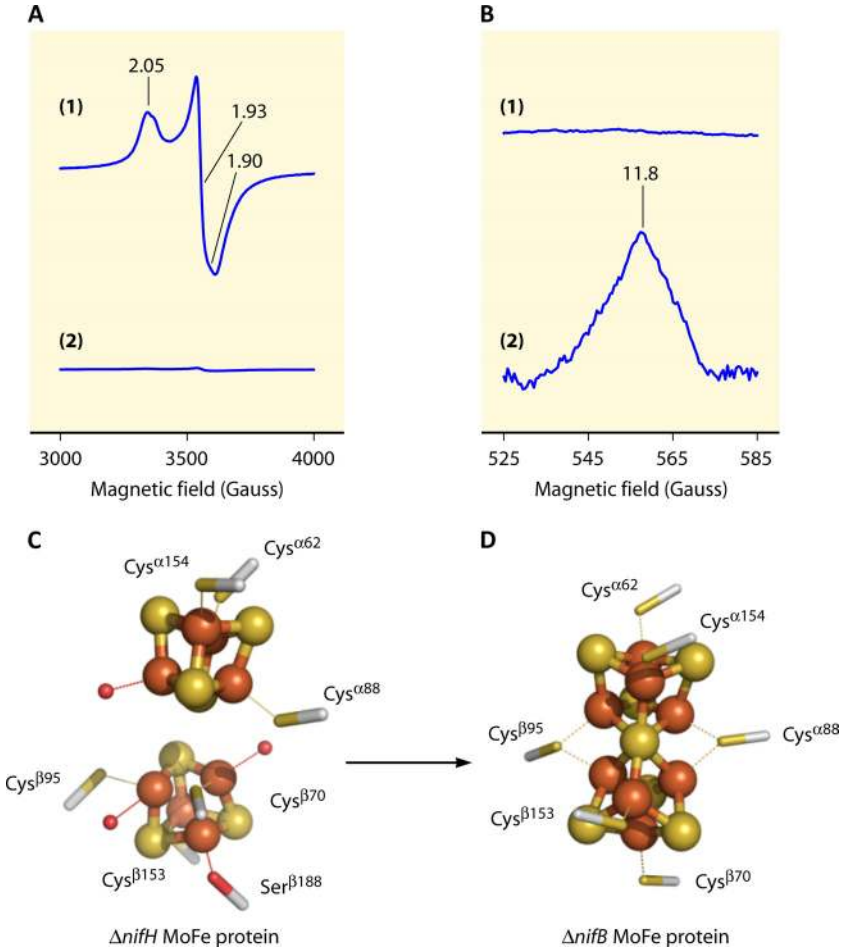

FIG. 10. (A and B) EPR spectra of the cluster species of Δ*nifH* MoFe protein in dithionite-reduced (A) and IDS-oxidized (B) states before (trace 1) and after (trace 2) maturation. The $S = 1/2$ signal at $g = 2.05$, 1.93, and 1.90 (A1), which is characteristic of the P-cluster precursor (i.e., paired $[Fe_4S_4]$ clusters), disappears upon maturation (A2), whereas the $g = 11.8$ parallel-mode signal (B2), which is characteristic of the mature P-cluster (i.e., $[Fe_8S_7]$ cluster in the P^{ox} state), emerges in the originally featureless region (B1) upon maturation. (C and D) Conversion of a pair of $[Fe_4S_4]$-like clusters (C) to a mature $[Fe_8S_7]$ P-cluster (D). The paired clusters comprise one standard $[Fe_4S_4]$ cubane (C, top) and one $[Fe_4S_4]$-like fragment that is distorted and/or coordinated by additional light atoms (C, bottom), which can be reductively coupled into a $[Fe_8S_7]$ structure (D) upon incubation with Fe protein, MgATP, and dithionite. The clusters are shown as ball-and-stick models, with the atoms colored as in Fig. 1, and the ligands are shown in stick presentation. PYMOL was used to create the figure.

circular dichroism (MCD) analyses provide further support for the unbridged model of the P-cluster in the Δ*nifH* MoFe protein, showing that each $[Fe_4S_4]$ cluster pair consists of an $[Fe_4S_4]^{1+}$ cluster and a diamagnetic $[Fe_4S_4]$-like cluster (3).

The $[Fe_4S_4]$-like cluster pair in the Δ*nifH* MoFe protein represents a physiologically relevant precursor to the P-cluster, as it can be converted to a mature P-cluster *in vitro* upon incubation with the Fe protein, MgATP, and dithionite (36). Upon maturation, the precursor-specific $S = 1/2$ signal disappears (Fig. 10A, trace 2), whereas the P-cluster (P^{2+})-specific $g = 11.8$ signal emerges (Fig. 10B, trace 2). These spectroscopic changes are accompanied by an increase in the reconstituted activity of the protein (36), both suggesting the conversion of precursors (Fig. 10C) to mature P-clusters (Fig. 10D) in this process. The real-time maturation of P-cluster can also be monitored by XAS/EXAFS analyses of the Δ*nifH* MoFe protein reisolated from the *in vitro* maturation assay after varying lengths of incubation time. The Fe K-edge XAS spectrum of the reisolated Δ*nifH* MoFe protein shows a clear shift over the duration of incubation in the shoulder feature of the rising edge at 7,117 eV, which corresponds to a successive reduction of cluster Fe atoms that eventually stabilize, on average, at a nearly all-ferrous oxidation state (36). The Fourier transforms of the EXAFS data show a shift in the first transform peak (at ~1.9 Å) to a longer distance, suggesting an elongation of the average Fe/S backscattering distance with longer incubation time, whereas the second Fourier transform peak (at ~2.4 Å) undergoes a substantial change in shape and intensity, reflecting a change in the Fe-Fe backscattering components during the course of incubation (36). Such a Fourier transform pattern is consistent with the conversion of the precursor to a mature P-cluster and provides strong proof that the P-cluster is formed through the reductive coupling of a pair of $[Fe_4S_4]$-like clusters.

The maturation of P-cluster is strictly ATP dependent; furthermore, it is maximized at specific reductant (dithionite) and reductase (Fe protein) concentrations, suggesting a key role of

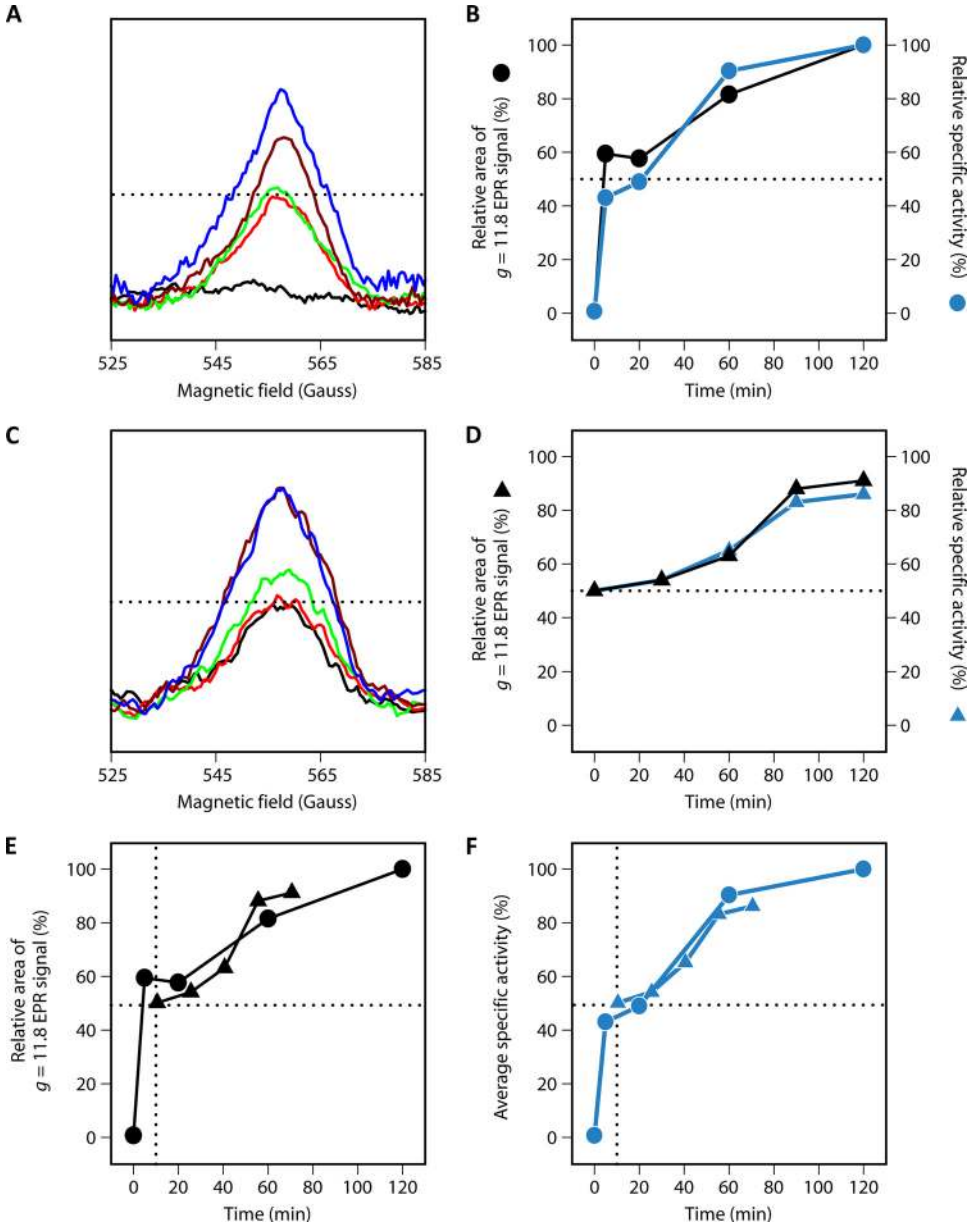

FIG. 11. (A and C) Emergence of the $g = 11.8$ parallel-mode EPR signal in the Δ*nifH* MoFe protein (A) and the Δ*nifB* Δ*nifZ* MoFe protein (C) over a certain time period. For A: black, 0 min; red, 5 min; green, 20 min; brown, 60 min; and blue, 120 min. For C: black, 0 min; red, 15 min; green, 30 min; brown, 45 min; and blue, 60 min. (B and D) Alignment of the time-dependent increase of the relative area of the $g = 11.8$ signal (blue) with that of the relative specific activity (black) of the Δ*nifH* MoFe protein (B) and the Δ*nifB* Δ*nifZ* MoFe protein (D). (E and F) Alignment of the time-dependent increase of the relative area of the $g = 11.8$ signal (E) and that of the relative specific activities (F) of the Δ*nifH* MoFe protein (solid circles) and the Δ*nifB* Δ*nifZ* MoFe protein (solid triangles). The horizontal dotted lines (A to F) represent the assembly of the first P-cluster (or half P-cluster content) in the MoFe protein, whereas the vertical dotted lines (E and F) mark the starting points for the alignment of data of the Δ*nifH* and Δ*nifB* Δ*nifZ* MoFe proteins.

redox chemistry in this process (36). These observations point to a third role of Fe protein, one that is crucial for the biosynthesis of P-cluster in the capacity of an ATP-dependent reductase. It is possible that the Fe protein acts in a similar manner in P-cluster assembly and substrate turnover, both of which involve the docking of the Fe protein on the MoFe protein, the conformational rearrangement of the two proteins, and the electron transfer between them; only in the case of P-cluster assembly, the Fe protein is specifically required for the redox tuning and the proper positioning of $[Fe_4S_4]$-like cluster pairs for their subsequent coupling.

Stepwise Assembly of the Two P-Clusters in MoFe Protein

The maturation of P-clusters in the Δ*nifH* MoFe protein follows an interesting biphasic pattern (36). The increase in the magnitude of the P^{2+}-specific signal (Fig. 11A and B, black line) aligns well with the increase in the activity of the

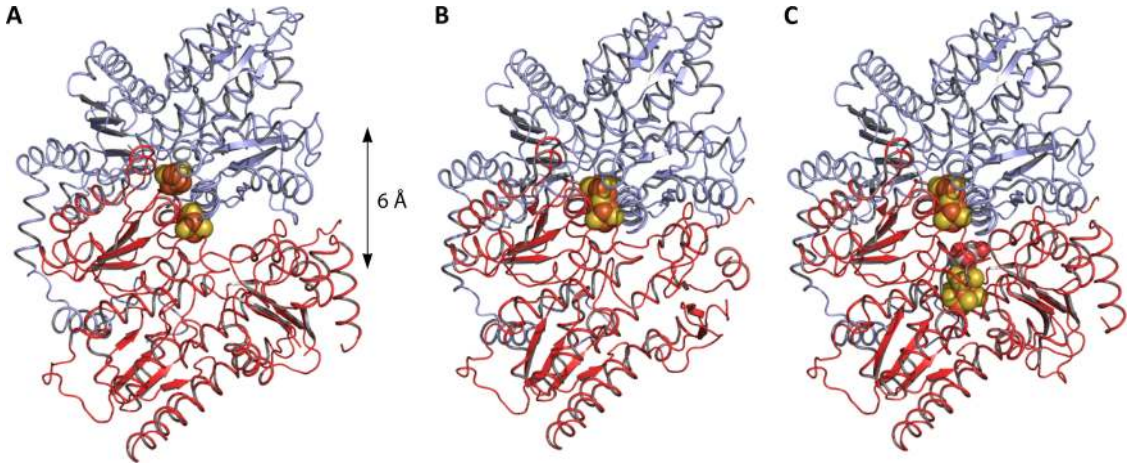

FIG. 12. Ribbon diagrams of the αβ-dimers of the Δ*nifH* MoFe protein (A), the Δ*nifB* MoFe protein (B), and the wild-type MoFe protein (C). The diagram in panel A represents the best model for Δ*nifH* MoFe protein based on SAXS data (8), which was constructed from the structure of the wild-type MoFe protein by deletion of the FeMoco, followed by a symmetric 6-Å translation of the α- and β-subunits about the *y* axis. The subunits and atoms are colored as in Fig. 1. PYMOL was used to create the figure (PDB entries 1M1N and 1L5H).

protein (Fig. 11B, blue line), both showing a lag period at approximately 50% of their respective maximum values (Fig. 11B, dotted line). Such a lag phase marks the formation of approximately half of the P-clusters in the protein, and given the presence of two P-clusters in the $\alpha_2\beta_2$-tetrameric MoFe protein, it may very well represent the completion of P-cluster assembly in the first αβ half of the protein. Consistent with the biphasic changes in the spectroscopic feature and enzymatic activity of the Δ*nifH* MoFe protein over the course of P-cluster maturation, the shift of Fe K-edge energy is unevenly paced, displaying a lack of significant energy shift in the lag period (36). EXAFS fit results further demonstrate a sequential rearrangement of the P-cluster species in the Δ*nifH* MoFe protein, showing a change in the ratio of short to long Fe-Fe distance in two distinct steps (36). Collectively, these observations provide dynamic proofs for the stepwise assembly mechanism of the two P-clusters in the MoFe protein, suggesting that the P-cluster in one αβ-dimer is formed prior to the other in the second αβ-dimer (Fig. 10).

A MoFe protein with only half P-cluster content (designated the Δ*nifB* Δ*nifZ* MoFe protein) can be captured upon the deletion of *nifB* and *nifZ* genes of *A. vinelandii* (25). Biochemical and MCD analyses show that the Δ*nifB* Δ*nifZ* MoFe protein contains a P-cluster in one αβ-dimer and a precursor like that found in the Δ*nifH* MoFe protein in the other αβ-dimer (10, 25). Moreover, the precursor in the second αβ-dimer of the Δ*nifB* Δ*nifZ* MoFe protein can also be converted to a fully matured P-cluster, showing a doubling of the magnitude of the P^{2+} signal (Fig. 11C and D, black line) that aligns well with the doubling in the activity of the protein (Fig. 11D, blue line). Interestingly, this conversion is well matched with the formation of the second P-cluster in the Δ*nifH* MoFe protein with regard to both the appearance of the P^{2+}-signal (Fig. 11E) and the increase of the activity (Fig. 11F). Thus, the permanent conformation of the Δ*nifB* Δ*nifZ* MoFe protein seems to be equivalent to the transient snapshot of the Δ*nifH* MoFe protein in the lag phase. There are, however, differences between the requirement for the maturation of the second P-clusters in the two MoFe proteins: the Δ*nifB* Δ*nifZ* MoFe protein requires the concerted actions of NifZ and Fe protein (26), whereas the Δ*nifH* MoFe protein requires only the action of Fe protein (36). This observation is not too surprising, as the Δ*nifH* MoFe protein is expressed in a *nifZ*-intact background and, therefore, has already "seen" the action of NifZ. The exact function of NifZ is not clear, although it has been proposed that NifZ may act in a chaperone-like function in the P-cluster maturation process (25, 26). Regardless, it is clear that NifZ is an essential factor for the assembly of the second P-cluster and, together with the Fe protein, it defines a unique, unsynchronized assembly mechanism of the two P-clusters in the MoFe protein.

Coordinated Assembly Events upon P-Cluster Maturation

The maturation of P-clusters sets off a series of coordinated assembly events of the MoFe protein. The stepwise formation of P-clusters renders a sequential maturation pattern of the two αβ halves of the MoFe protein. Furthermore, the coupling of the two $[Fe_4S_4]$-like subclusters at each α/β-subunit interface likely provides added stability to the αβ-dimer of the MoFe protein. This argument is supported by the comparative SAXS analysis of the Δ*nifH*, the Δ*nifB*, and the wild-type MoFe proteins, showing that the Δ*nifH* MoFe protein exists in the most extended conformation (R_g = 45.7 Å), followed by the Δ*nifB* MoFe protein (R_g = 42.4 Å) and then the wild-type MoFe protein (R_g = 40.2 Å) (8). The increase in the size of the Δ*nifH* MoFe protein is correlated to an increase in the solvent accessibility of the Fe atoms of the P-cluster precursors and can be best modeled by a 6-Å gap at the α/β-subunit interface (Fig. 12A) that is absent from the structure of either the Δ*nifB* (Fig. 12B) or the wild-type (Fig. 12C) MoFe protein. These results suggest that the coupling of the $[Fe_4S_4]$ subclusters is accompanied by a conformational change that brings the α- and β-subunits of the MoFe protein together. Apart from its effect on the α/β-subunit interface, the process of P-cluster

assembly also impacts the FeMoco binding site within the α-subunit of MoFe protein. Prior to the maturation of P-clusters, the FeMoco sites in the Δ*nifH* MoFe protein assume a closed conformation that does not allow cofactor insertion. During the course of P-cluster maturation, however, the FeMoco sites are gradually opened up, till they acquire the same open conformation as that of the FeMoco sites in the Δ*nifB* MoFe protein (48). The Fe protein is likely responsible for inducing the conformational changes in this process, interacting with the MoFe protein in a manner similar to that during the substrate turnover of nitrogenase; more importantly, it plays a pivotal role in orchestrating the multiple assembly events that eventually lead to the formation of a mature MoFe protein.

THE PARALLELISM BETWEEN FeMoco AND P-CLUSTER ASSEMBLY

There is a certain parallelism between the biosynthetic routes of FeMoco and P-cluster, as the assembly of both clusters involves the fusion of two 4Fe fragments into an 8Fe entity. Compared to the assembly of P-cluster, the assembly of FeMoco is clearly more complicated, entailing the insertion of an additional S atom and (perhaps) the interstitial X atom, the rearrangement of the Fe/S core in the "waist" area, and the replacement of one terminal Fe by Mo and homocitrate. The fact that the core of FeMoco undergoes more processing steps than that of the P-cluster may account for the more elaborate *ex situ* synthetic route of the former and the less complicated *in situ* synthetic route of the latter. Nevertheless, the common usage of paired 4Fe building blocks for Fe/S core construction renders a topological resemblance between the two clusters. Such a similarity has been well illustrated by the chemically synthesized FeMoco and P-cluster topologs, which can be obtained through the rearrangement of similar core structures (39, 58).

Comparison between the cluster compositions of NifEN and MoFe protein further implies a parallel evolutionary pattern of these topologically associated clusters. Better known for its function as a scaffold protein for FeMoco maturation (see above), NifEN is also a catalytic homolog of the MoFe protein, although it is capable of reducing only a limited range of substrates at a considerably lower efficiency (31). Given that NifEN contains the respective precursor forms of the two clusters in the MoFe protein, a coevolution theory can be proposed for the P-cluster and FeMoco—one that involves the function- and locale-dependent structural rearrangements of clusters sharing the same topology. Further examination of the P-cluster and FeMoco assembly pathways is under way, which will provide additional insights into the mechanism and evolution of nitrogenase.

ACKNOWLEDGMENT

This work was supported by National Institutes of Health grant GM-67626 (M.W.R.).

REFERENCES

1. **Allen, R. M., R. Chatterjee, P. W. Ludden, and V. K. Shah.** 1995. Incorporation of iron and sulfur from NifB cofactor into the iron-molybdenum cofactor of dinitrogenase. J. Biol. Chem. **270:**26890–26896.
2. **Brigle, K. E., M. C. Weiss, W. E. Newton, and D. R. Dean.** 1987. Products of the iron-molybdenum cofactor-specific biosynthetic genes, *nifE* and *nifN*, are structurally homologous to the products of the nitrogenase molybdenum-iron protein genes, *nifD* and *nifK*. J. Bacteriol. **169:**1547–1553.
3. **Broach, R. B., et al.** 2006. VTVH-MCD spectroscopic study of the metal clusters in the Δ*nifB* and Δ*nifH* MoFe proteins of nitrogenase from *Azotobacter vinelandii*. Biochemistry **45:**15039–15048.
4. **Burgess, B. K.** 1990. The iron molybdenum cofactor of nitrogenase. Chem. Rev. **90:**1377–1406.
5. **Burgess, B. K., and D. J. Lowe.** 1996. Mechanism of molybdenum nitrogenase. Chem. Rev. **96:**2983–3012.
6. **Chan, M. K., J. Kim, and D. C. Rees.** 1993. The nitrogenase FeMo-cofactor and P-cluster pair: 2.2 Å resolution structures. Science **260:**792–794.
7. **Corbett, M. C., et al.** 2006. Structural insights into a protein-bound iron-molybdenum cofactor precursor. Proc. Natl. Acad. Sci. U. S. A. **103:**1238–1243.
8. **Corbett, M. C., et al.** 2007. Conformational differences between *Azotobacter vinelandii* nitrogenase MoFe proteins as studied by small angle X-ray scattering. Biochemistry **46:**8066–8074.
9. **Corbett, M. C., et al.** 2004. Comparison of iron-molybdenum cofactor deficient nitrogenase MoFe proteins by X-ray absorption spectroscopy: implications for P-cluster biosynthesis. J. Biol. Chem. **279:**28276–28282.
10. **Cotton, M. S., et al.** 2009. VTVH-MCD study of the Δ*nifB*Δ*nifZ* MoFe protein from *Azotobacter vinelandii*. J. Am. Chem. Soc. **131:**4558–4559.
11. **Dean, D. R., and M. R. Jacobson.** 1992. Biochemical genetics of nitrogenase, p. 763–834. *In* G. Stacey, R. H. Burris, and H. J. Evans (ed.), Biological nitrogen fixation. Chapman and Hall, New York, NY.
12. **Einsle, O., et al.** 2002. Nitrogenase MoFe-protein at 1.16 Å resolution: a central ligand in the FeMo-cofactor. Science **297:**1696–1700.
13. **Fay, A. W., et al.** 2011. Spectroscopic characterization of the isolated iron-molybdenum cofactor (FeMoco) precursor from the protein NifEN. Angew. Chem. Int. Ed. Engl. **50:**7787–7790.
14. **Fay, A. W., et al.** 2010. Formation of a homocitrate-free iron-molybdenum cluster on NifEN: implications for the role of homocitrate in nitrogenase assembly. Dalton Trans. **39:**3124–3130.
15. **Fay, A. W., Y. Hu, B. Schmid, and M. W. Ribbe.** 2007. Molecular insights into nitrogenase FeMoco insertion – the role of His 274 and His 451 of MoFe protein α subunit. J. Inorg. Biochem. **101:**1630–1641.
16. **Georgiadis, M. M., et al.** 1992. Crystallographic structure of the nitrogenase iron protein from *Azotobacter vinelandii*. Science **257:**1653–1659.
17. **Goodwin, P. J., et al.** 1998. The *Azotobacter vinelandii* NifEN complex contains two identical [4Fe-4S] clusters. Biochemistry **37:**10420–10428.
18. **Hernandez, J. A., et al.** 2008. Metal trafficking for nitrogen fixation: NifQ donates molybdenum to NifEN/NifH for the biosynthesis of the nitrogenase FeMo-cofactor. Proc. Natl. Acad. Sci. U. S. A. **105:**11679–11684.
19. **Hlavinka, M. L., T. Miyaji, R. J. Staples, and R. H. Holm.** 2007. Hydroxide-promoted core conversions of molybdenum-iron-sulfur edge-bridged double cubanes: oxygen-ligated topological P^N clusters. Inorg. Chem. **46:**9192–9200.
20. **Hoover, T. R., et al.** 1987. Identification of the V-factor needed for synthesis of the iron-molybdenum cofactor of nitrogenase as homocitrate. Nature **329:**855–857.
21. **Howard, J. B., and D. C. Rees.** 2006. How many metals does it take to fix N_2? A mechanistic overview of biological nitrogen fixation. Proc. Natl. Acad. Sci. U. S. A. **103:**17088–17093.
22. **Howard, J. B., and D. C. Rees.** 1996. Structural basis of biological nitrogen fixation. Chem. Rev. **96:**2965–2982.
23. **Hu, Y., et al.** 2006. FeMo cofactor maturation on NifEN. Proc. Natl. Acad. Sci. U. S. A. **103:**17119–17124.
24. **Hu, Y., et al.** 2006. Nitrogenase Fe protein: a molybdate/homocitrate insertase. Proc. Natl. Acad. Sci. U. S. A. **103:**17125–17130.
25. **Hu, Y., A. W. Fay, P. C. Dos Santos, F. Naderi, and M. W. Ribbe.** 2004. Characterization of *Azotobacter vinelandii nifZ* deletion strains - indication of stepwise MoFe protein assembly. J. Biol. Chem. **279:**54963–54971.
26. **Hu, Y., A. W. Fay, C. C. Lee, and M. W. Ribbe.** 2007. P-cluster maturation on nitrogenase MoFe protein. Proc. Natl. Acad. Sci. U. S. A. **104:**10424–10429.
27. **Hu, Y., A. W. Fay, C. C. Lee, J. M. Yoshizawa, and M. W. Ribbe.** 2008. Assembly of nitrogenase MoFe protein. Biochemistry **47:**3973–3981.
28. **Hu, Y., A. W. Fay, and M. W. Ribbe.** 2005. Identification of a nitrogenase iron-molybdenum cofactor precursor on NifEN complex. Proc. Natl. Acad. Sci. U. S. A. **102:**3236–3241.
29. **Hu, Y., A. W. Fay, and M. W. Ribbe.** 2007. Molecular insights into nitrogenase FeMoco insertion – the role of His362 of MoFe protein α subunit in FeMoco incorporation. J. Biol. Inorg. Chem. **12:**449–460.
30. **Hu, Y., A. W. Fay, B. Schmid, B. Makar, and M. W. Ribbe.** 2006. Molecular insights into nitrogenase FeMoco insertion - Trp 444 of MoFe protein α subunit locks FeMoco in its binding site. J. Biol. Chem. **281:**30534–30541.
31. **Hu, Y., et al.** 2009. Catalytic activities of NifEN: implications for nitrogenase evolution and mechanism. Proc. Natl. Acad. Sci. U. S. A. **106:**16962–16966.
32. **Joerger, R. D., and P. E. Bishop.** 1988. Bacterial alternative nitrogen fixation systems. Crit. Rev. Microbiol. **16:**1–14.
33. **Joerger, R. D., and P. E. Bishop.** 1988. Nucleotide sequence and genetic analysis of the *nifB-nifQ* region from *Azotobacter vinelandii*. J. Bacteriol. **170:**1475–1487.
34. **Kaiser, J. T., Y. Hu, J. A. Wiig, D. C. Rees, and M. W. Ribbe.** 2011. Structure

of precursor-bound NifEN: a nitrogenase FeMo cofactor maturase/insertase. Science **331:**91–94.
35. **Kim, J., and D. C. Rees.** 1992. Crystallographic structure and functional implications of the nitrogenase molybdenum iron protein from *Azotobacter vinelandii*. Nature **360:**553–560.
36. **Lee, C. C., et al.** 2009. Stepwise formation of P-cluster in nitrogenase MoFe protein. Proc. Natl. Acad. Sci. U. S. A. **106:**18474–18478.
37. **Lee, H.-I., B. J. Hales, and B. M. Hoffman.** 1997. Metal-ion valencies of the FeMo cofactor in CO-inhibited and resting state nitrogenase by Fe-57 Q.-band ENDOR. J. Am. Chem. Soc. **119:**11395–11400.
38. **Lee, S. C., and R. H. Holm.** 2004. The clusters of nitrogenase: synthetic methodology in the construction of weak-field clusters. Chem. Rev. **104:** 1135–1158.
39. **Ohki, Y., Y. Ikagawa, and K. Tatsumi.** 2007. Synthesis of new [8Fe-7S] clusters: a topological link between the core structures of P-cluster, FeMo-co, and FeFe-co of nitrogenases. J. Am. Chem. Soc. **129:**10457–10465.
40. **Ohki, Y., et al.** 2009. Synthesis, structures, and electronic properties of [8Fe-7S] cluster complexes modeling the nitrogenase P-cluster. J. Am. Chem. Soc. **131:**13168–13178.
41. **Ohki, Y., Y. Sunada, M. Honda, M. Katada, and K. Tatsumi.** 2003. Synthesis of the P-cluster inorganic core of nitrogenases. J. Am. Chem. Soc. **125:**4052–4053.
42. **Peters, J. W., et al.** 1997. Redox-dependent structural changes in the nitrogenase P-cluster. Biochemistry **36:**1181–1187.
43. **Pettersen, E. F., et al.** 2004. UCSF Chimera - a visualization system for exploratory research and analysis. J. Comput. Chem. **25:**1605–1612.
44. **Pierik, A. J., H. Wassink, H. Haaker, and W. R. Hagen.** 1993. Redox properties and EPR spectroscopy of the P-clusters of *Azotobacter vinelandii* MoFe protein. Eur. J. Biochem. **212:**51–61.
45. **Ribbe, M. W., Y. Hu, M. Guo, B. Schmid, and B. K. Burgess.** 2002. The FeMoco-deficient MoFe protein produced by a *nifH*-deletion strain of *Azotobacter vinelandii* shows unusual P-cluster features. J. Biol. Chem. **277:** 23469–23476.
46. **Rubio, L. M., and P. W. Ludden.** 2008. Biosynthesis of the iron-molybdenum cofactor of nitrogenase. Annu. Rev. Microbiol. **62:**93–111.
47. **Schindelin, H., C. Kisker, J. L. Schlessman, J. B. Howard, and D. C. Rees.** 1997. Structure of ADP · AlF_4^--stabilized nitrogenase complex and its implications for signal transduction. Nature **387:**370–376.
48. **Schmid, B., et al.** 2002. Structure of a cofactor-deficient nitrogenase MoFe protein. Science **296:**352–356.
49. **Schwarz, G., R. R. Mendel, and M. W. Ribbe.** 2009. Molybdenum cofactors, enzymes and pathways. Nature **460:**839–847.
50. **Shah, V. K., and W. J. Brill.** 1977. Isolation of an iron-molybdenum cofactor from nitrogenase. Proc. Natl. Acad. Sci. U. S. A. **74:**3249–3253.
51. **Smith, A. D., et al.** 2005. NifS-mediated assembly of [4Fe-4S] clusters in the N- and C-terminal domains of the NifU scaffold protein. Biochemistry **44:** 12955–12969.
52. **Surerus, K. K., et al.** 1992. Mössbauer and integer-spin EPR of the oxidized P-clusters of nitrogenase - P^{ox} is a non-kramers system with a nearly degenerate ground doublet. J. Am. Chem. Soc. **114:**8579–8590.
53. **Watt, G. D., A. Burns, S. Lough, and D. L. Tennent.** 1980. Redox and spectroscopic properties of oxidized MoFe protein from *Azotobacter vinelandii*. Biochemistry **19:**4926–4932.
54. **Wiig, J. A., Y. Hu, and M. W. Ribbe.** 2011. NifEN-B complex of *Azotobacter vinelandii* is fully functional in nitrogenase FeMo cofactor assembly. Proc. Natl. Acad. Sci. U. S. A. **108:**8623–8627.
55. **Yoo, S. J., H. C. Angove, V. Papaefthymiou, B. K. Burgess, and E. Münck.** 2000. Mössbauer study of the MoFe protein of nitrogenase from *Azotobacter vinelandii* using selective Fe^{57} enrichment of the M-centers. J. Am. Chem. Soc. **122:**4926–4936.
56. **Yoshizawa, J. M., et al.** 2009. Optimization of FeMoco maturation on NifEN. J. Am. Chem. Soc. **131:**9321–9325.
57. **Zhang, Y., and R. H. Holm.** 2004. Structural conversions of molybdenum-iron-sulfur edge-bridged double cubanes and P^N-type clusters topologically related to the nitrogenase P-cluster. Inorg. Chem. **43:**674–682.
58. **Zhang, Y., and R. H. Holm.** 2003. Synthesis of a molecular $Mo_2Fe_6S_9$ cluster with the topology of the P^N cluster of nitrogenase by rearrangement of an edge-bridged $Mo_2Fe_6S_8$ double cubane. J. Am. Chem. Soc. **125:**3910–3920.
59. **Zhang, Y., J. L. Zuo, H. C. Zhou, and R. H. Holm.** 2002. Rearrangement of symmetrical dicubane clusters into topological analogues of the P cluster of nitrogenase: nature's choice? J. Am. Chem. Soc. **124:**14292–14293.
60. **Zheng, L. M., R. H. White, and D. R. Dean.** 1997. Purification of the *Azotobacter vinelandii nifV*-encoded homocitrate synthase. J. Bacteriol. **179:** 5963–5966.
61. **Zimmermann, R., et al.** 1978. Nitrogenase X: Mössbauer and EPR studies on reversibly oxidized MoFe protein from *Azotobacter vinelandii* OP. Nature of iron centers. Biochim. Biophys. Acta **537:**185–207.

Yilin Hu received a B.S. degree in Genetics from Fudan University, China, and a Ph.D. degree in Biochemistry from Loma Linda University. She was a postdoctoral fellow at the University of California, Irvine and is currently associate project scientist at the same institute. During the last 10 years, she has been focusing on studies related to nitrogenase mechanism and assembly, with an emphasis on the genetic manipulation of nitrogenase systems.

Markus W. Ribbe received a B.S. degree in Biology, a M.S. degree in Microbiology, and a Ph.D. degree in Microbiology from the University of Bayreuth, Germany. He was a postdoctoral fellow at the University of California, Irvine and is now professor at the same institute. During the past 15 years, he has been focusing on the mechanistic investigation of nitrogenase catalysis and assembly by combined biochemical, spectroscopic, and structural approaches.